

Characterization of the Photoacid Diffusion Length and Reaction Kinetics in EUV Photoresists with IR Spectroscopy

Shuhui Kang,^{*,†} Wen-li Wu,[†] Kwang-Woo Choi,^{†,‡} Anuja De Silva,[§] Christopher K. Ober,[§] and Vivek M. Prabhu^{*,†}

[†]Polymers Division, National Institute of Standards and Technology, 100 Bureau Dr, Gaithersburg, Maryland 20899, [‡]Intel Corporation, Santa Clara, California 95054-1549, and [§]Cornell University, Materials Science & Engineering, 310 Bard Hall, Ithaca, New York 14853-1501

Received November 19, 2009; Revised Manuscript Received March 16, 2010

ABSTRACT: A soft-contact film transfer method was developed to prepare multilayer photoresist thin films that enable high-resolution spectroscopic and reflectivity measurements for determining the reaction–diffusion kinetic parameters and photoacid diffusion length. Infrared reflectance absorption spectroscopy was applied to follow, quantitatively, the reaction–diffusion kinetics during the post-exposure bake (PEB) step; the time evolution of the average deprotection level across a bilayer film with model photoresists is described by a kinetics model with three parameters: a reaction rate constant (k_p), the phenomenological photoacid trapping constant (k_T), and the photoacid diffusion constant (D_H). A polymeric and molecular resist for next-generation extreme ultraviolet (EUV) lithography with chemically analogous structure was studied with this methodology. The three kinetic parameters follow an Arrhenius dependence but show quantitative differences between these two photoresists at a given PEB temperature. Further it was demonstrated that the photoacid diffusion length is not a simple function of diffusion coefficient; instead, it is dictated by all three kinetics parameters jointly in addition to the deprotection level at which the resist becomes soluble in an aqueous developer solution. These observations qualitatively explain the experimentally observed shorter photoacid diffusion length of the molecular resist in comparison to its polymeric counterpart.

1. Introduction

Photoresist materials enable the fabrication of advanced integrated circuits with ever-decreasing feature sizes. As next-generation light sources are developed, using extreme ultraviolet light of wavelength 13.5 nm, photoresist formulations must meet strict image-fidelity criteria in order to maintain the expected performance in feature size reduction or resolution. The quality of the patterned structures depends upon sequential process steps that influence the spatial distribution of either the photoacids or photoacid-catalyzed reaction–diffusion process.^{1,2} The relationships between the initial optical exposure and the feature quality are specifically controlled by the reaction–diffusion of the photoacid^{3–5} into nominally unexposed regions. This image spreading or blurring is caused by photoacid diffusion.^{6,7} Controlling the reaction–diffusion process remains the predominant strategy to achieve resolution (critical dimension, CD)^{8–12} and line-edge roughness (LER), metrics for the ultimate resolution of a printed feature. Since the photoacid diffusion length (L_d) must generally be reduced to lengths smaller than the expected feature size ($L_d < CD$), the characterization of the reaction–diffusion kinetics and photoacid diffusion length becomes increasingly important to photolithography technology.

In any lithographic study the measured CD is a function of numerous process and formulation conditions that have been optimized. Subsequently, analysis of scanning electron microscopy (SEM) images provides a direct measure of final resolution and LER. A particular challenge has been to develop quantitative models with physical parameters to calculate full three-dimensional

features. Commercial programs often benchmark parameters based upon lithographically defined line and space features. However, interpreting parameters from independent experiments in terms of variables traceable to basic chemical reaction–diffusion equations and or phenomenological parameters has seen recent interest as the desired feature sizes have appeared to reach their resolution limits. One variable of particular importance is the photoacid diffusion length. While the photoacid is an ionic species and therefore should follow the diffusion of an electrolyte,¹³ most experimental data treat the photoacid a single species rather than the coupled diffusion with distinct diffusivities of the proton and counteranion.

In order to reduce the photoacid diffusion length, one may develop methods to restrict the diffusivity, such as increasing the molar mass or operating at lower temperatures relative to the glass transition.^{14–17} In some cases the effect of film confinement was attributed to reduced diffusivity via the change in physico-chemical properties.^{18,19} However, photoresist films are not inert layers but undergo simultaneous reaction and diffusion.³ The presence of diffusing small molecules catalyzes the additional chemical reaction which drastically changes the polarity of the matrix^{10,16,20–23} as the volatile reaction products leave the film or less fugitive products may modify the local viscoelastic properties. This raises fundamental issues regarding the validity of a single diffusion constant in a glassy medium,^{16,20} the influence of a changing density or glass transition temperature, and the role of multicomponent mixtures on the effective diffusion of a low molar mass species. In this paper we extend a phenomenological model to understand experimental data regarding the complex reaction–diffusion process. We demonstrate that a diffusion equation combined with simple reaction is insufficient to model the experimental data. Phenomenologically, a process

*Corresponding authors: e-mail shuhui.kang@nist.gov, tel 301-975-4602, fax 301-975-3928 (S.K.); e-mail vprabhu@nist.gov, tel 301-975-3657, fax 301-975-3928 (V.M.P.).

that reduces the availability or efficiency of photoacids is required in a spatially dependent and reaction-time-dependent manner. This is referred to as a photoacid trapping process, whereby the trapping rate is proportional to the trapping constant and first order in photoacid concentration and polar reactant products. A scheme is experimentally developed to provide a quantification of the photoacid diffusion length in the absence of a model, but based upon measurable film thickness.

The basics of diffusion are rooted in Brownian motion whereby the mean-square displacement is governed by the number of steps and effective step length, $\langle R^2 \rangle = NL_d^2$ or, equivalently, the diffusion constant and time, $\langle R^2 \rangle = 6Dt$. In photoresist materials the diffusion length is generally defined by $(2Dt)^{1/2}$, where the D is the apparent diffusion coefficient of photoacid in a photoresist and the t is the time permitted for the reaction–diffusion process. However, despite the convenience of this analysis, the quantification of diffusion length in the real situation is more complicated. First, a direct measurement of the diffusion coefficient of the photoacid is extremely difficult not only because the concentration of photoacid is very low, resulting in low sensitivity, but also because the photoacid is a catalyst that reacts with the surrounding photoresist. Therefore, the photoresist properties are changing as a function of time. The diffusion coefficient of the photoacid is always inferred by a kinetics model through the measurement of its reaction products. Second, the diffusion length obtained by this process is not necessarily relevant to the actual situation. For instance, the point-spread function simultaneously provides the characteristic diffusion length and extent of reaction. This approach was enabled by interferometric lithography to characterize and compare different resists.^{11,24} Also, the diffusion distance a photoacid travels from the nominally exposed region to the unexposed region provides an estimate of the ultimate resolution caused by image slimming after development. However, this may not reflect any relationship to $(2Dt)^{1/2}$ even under ideal optical exposure conditions.

Transport fundamentals have a long-standing interest in polymer science. The diffusion constant in polymer and block copolymer melts may be determined by measurements of interdiffusion.^{25–28} This was enabled by the preparation of bilayer and multilayer films with nanometer initial interfacial width. The thermally activated interdiffusion led to well-defined concentration profiles that were used to test models for polymer diffusion. Recently, Torkelson et al.^{29,30} and Ediger et al.³¹ applied sophisticated fluorescence and neutron reflectivity methods on specially prepared thin film multilayers to probe dynamic heterogeneity and confinement effects near the glass transition. Ober et al. found that photoacid exchange and diffusion processes were critical to organic electronic device fabrication and performance of the fabrication of light-emitting polymer devices.³² Of specific interest to photoacid diffusion, quantification methods of photoacid diffusion coefficients or diffusion length are available. These methods may use a single resist thin film, a bilayer or trilayer of resist with a photoacid generator feeding layer. In the case of multilayers the photoacid formed by exposure would diffuse in the thin glassy polymer film and be detected by the extent of reaction.

A novel approach was developed by Houle and IBM co-workers^{16,20} to measure reaction kinetics. They use a photoresist thin film containing PAG and expose to a UV wavelength that is strongly absorbed by the film, such that effectively only the surface is exposed, not the entire film. Therefore, subsequent processing has the characteristics of one-dimensional photoacid diffusion gradient in this *in situ* formed photoacid layer. This approach has several advantages: the photoacid diffuses within one resist media, which is close to real situation in lithography; a variety of systems and formulations may be rapidly examined, so long as the film remains highly UV absorbing. The initial

photoacid profile depends upon the film absorbance characteristics that was determined by combined stochastic modeling and FTIR measurements.

Previous bilayer stack methods used different polymer films, typically a resist and a polymer film loaded with PAG. This bilayer is then exposed to UV light forming photoacid in PAG-containing layer.^{17,33–36} Since the bilayer consists of two different polymers, the main drawback was that the photoacid diffusion could be different in each layer. This may impose difficulties in modeling and interpretation. A trilayer stack method in which the studied resist is sandwiched between an acid feeding layer and a detection layer has also been used.³⁷ This approach required floating films from water.

In this paper, we propose a new method to prepare multilayer films made by a soft-contact film transfer technique.³⁸ This approach resolves two major hurdles over conventional methods to prepare multilayers: multilayers of the same polymer film are traditionally prepared by floating a second film on the surface of water.³⁹ However, this approach is plagued by partial dissolution of film additives as well as limited by fragile films that crumble under the surface tension of water. These two issues can prevent quantitative analysis and limit measurement methods that require large uniform areas. Multilayers of different polymer films may be prepared by sequential spin-coating. However, this is limited to finding satisfactory solvent/nonsolvent pairs.⁴⁰ Bilayers of arbitrary polymer thin films using the soft-contact film transfer approach developed here resolve these frequently encountered problems.

We apply this approach to study the photoacid diffusion length and reaction kinetics in molecular glass resists. The PAG is loaded in the top layer of the bilayer film, but both the top and bottom layer are the same resist. This provides one diffusion medium for the photoacid that resolves a previous challenge. Since the PAG is restricted to one layer, the photoacid distribution is well-defined by the bilayer, and one may use the specific wavelength of interest for exposure, such as EUV whereby the photoacid generation mechanisms are different than UV.⁴¹ Large uniform areas, such as 76 mm diameter wafers, prepared by our methods are amenable to a variety of high-resolution techniques such as X-ray and neutron reflectivity and spectroscopy ellipsometry. In the present study, a nondestructive FTIR measurement with a hot stage is used to collect the data in real time. The samples after postexposure bake (PEB) were then developed in an aqueous hydroxide solution, and the etching depth was measured in comparison to model predictions.

With the method established, we studied two model EUV photoresists: a poly(hydroxystyrene-*co-tert*-butyl acrylate) that bears resemblance to the commercial environmentally stable chemically amplified photoresist (ESCAP) and a novel calix[4]resorcinarene molecular glass (MG) resist. Since the CD and LER metrics are approaching the characteristic dimensions of the photoresist polymers, alternative architectures were considered to extend photolithography by using lower molar mass molecules.⁴² These molecular glass resists, while smaller, may also improve the uniformity of blends with PAG and other additives.⁴³ The MG resists may also benefit from a more uniform development due to the lack of chain entanglements and long relaxation times, essentially eliminating swelling, when compared to polymers. Molecular glass resists have a well-defined core with pendant protected base-soluble groups (such as hydroxyls and carboxyls). With this approach the core chemistry can vary from ringlike calix[4]resorcinarenes,^{44–47} branched phenolic groups,^{48,49} and disklike hexaphenolic groups.^{50,51} Early approaches with MG led to low glass transition temperatures; however, such problems were resolved by increased hydrogen-bonding functionality and design of the core structure. High glass transition temperatures (typically, $T_g > 140$ °C with polymers) provide dimensional stability.

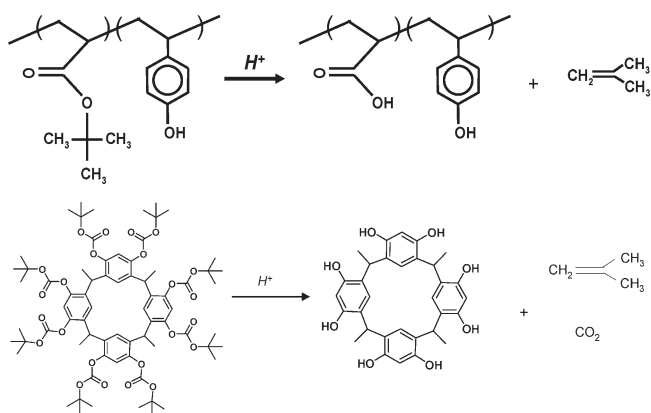


Figure 1. Acid-catalyzed (H^+) deprotection reaction of (a) P(HOST-*co*-tBA) and (b) t-BOC-protected calix[4]resorcinarene.

These approaches follow the chemically amplified photoresist blend approach with critical additives.

While these new materials are under active lithographic testing, quantitative measurements of photoacid diffusion length, latent-image log slope, and dose sensitivity are lacking. In this work, we compare the deprotection reaction–diffusion kinetics of a common photoacid generator in a polymer and molecular glass resist with similar resist chemistry to characterize basic effects of molecular architecture on the photoacid diffusion length and reaction–diffusion front. Such a comparison is very important because the photoacid catalyzed deprotection reaction is the root cause of current projection lithography feature limitations. Measurements of the reaction kinetics constants and photoacid diffusion constant would allow a predictive approach to line-edge feature critical dimensions and LER. This approach will provide parameters that may qualify, or aid in the interpretation or benchmark parameters determined by photolithography process window experiments.

2. Experimental Section⁷⁹

2.1. Materials. Two different architectures of resists—a polymer photoresist, poly(hydroxystyrene-*co*-*tert*-butyl acrylate) or P(HOST-*co*-tBA),⁵² and a *tert*-butoxycarbonyl (t-BOC)-protected tetra-C-methylcalix[4]resorcinarene (CM4R) molecular glass material—were studied.⁵³ The P(HOST-*co*-tBA) had a number-average relative molar mass (M_n) = 11 460 g/mol, polydispersity index (PDI) = 1.8, and copolymer composition of 49 mol % hydroxystyrene and 51 mol % *tert*-butyl acrylate (DuPont Electronic Polymers). The chemical formula and photoacid-catalyzed deprotection reaction equation are shown in Figure 1. The same photoacid generator, triphenylsulfonium perfluorobutanesulfonate (TPS-PFBS), was used to directly compare the effect of molecular architecture on the photoacid reaction–diffusion kinetics. When referring to the PAG loadings (or concentration), it will be implied as mass % of resist from this point forward. We notice that the protection groups differ, which will lead to a small difference in activation energy of the reaction; however, both materials share the phenol functionality. We will compare our results to those in the literature for t-BOC-protected PHOST which share the same protection chemistry as the molecular resist studied in this paper.

2.2. Bilayer Process: Soft-Contact Film Transfer. In this study we use two methods of thin film preparation: single layer and bilayer. The single-layer method refers to the photoresist formulation (resist + PAG blend) prepared on a silicon wafer. The bilayer method involves forming a stacked layer structure of two films on a silicon wafer with well-defined thickness and no intermixing. Both single layer and bilayer films are used in this experiment. In the single layer film, the PAG is uniformly

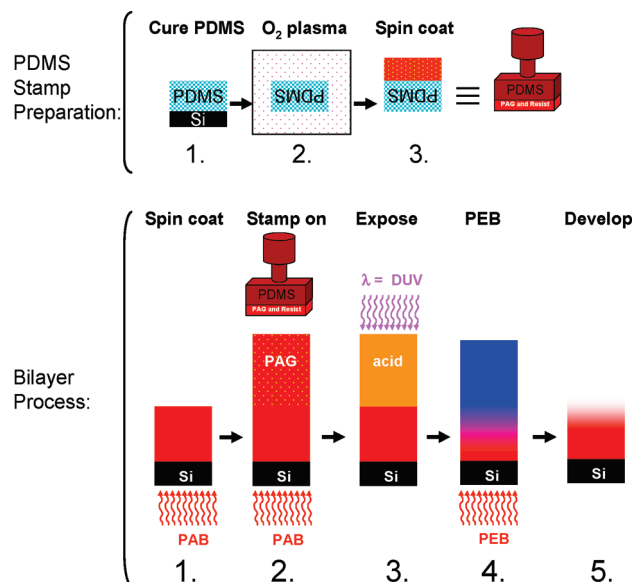


Figure 2. Bilayer sample preparation with the PDMS film stamping technique.

distributed, while in the bilayer film, the PAG is present only in the top layer. The single layer sample provides the simplest system to study the reaction kinetics and estimate the reaction rate constant and photoacid trapping rate constant. In the single layer film, the diffusion coefficient is completely coupled with the reaction rate constant because the gradient of photoacid concentration is zero. In order to determine the photoacid diffusion coefficient, a well-defined initial acid gradient is necessary to follow the moving photoacid reaction front.

A new film stamping technique (Figure 2) was developed to generate the well-defined step acid concentration gradient.³⁸ In this case a resist film containing PAG is prepared on a poly(dimethylsiloxane) (PDMS) substrate and then stamped onto an PAG-free resist film at an elevated temperature. After the stack cools the PDMS substrate is removed. The primary advantage of this bilayer approach is that only one diffusion medium is present. This approach is more convenient than double spin-coating methods that provide high-fidelity bilayers but is limited with respect to finding suitable casting solvents for the acid feeder layers that do not share the same polymer media as the bottom layer.^{17,33,54} The PDMS method is capable of forming a sharp interface between two identical polymer layers. However, in our case the top layer contains PAG. The interfacial width was between 1 nm to 2 nm as measured by neutron reflectivity with a bilayer of deuterated and protonated poly(methyl methacrylate). Therefore, the loaded PAG has a nearly perfect step profile within length scales of the interfacial width.

One of the most important steps in our approach is to make a bilayer film consisting of only one resist but with PAG located at the top or bottom layer film. This design simplifies the experiment and modeling because the initial PAG distribution is defined by a sharp interface between the top and bottom layers, and the transport properties are across the same medium. This is a large improvement over all previous approaches.

The procedure for preparing these bilayer films involves three major steps: spin-coating of bottom layer, stamp fabrication, and stamp film transfer. The bottom layer film that does not contain PAG should be prepared beforehand onto clean silicon wafers and postapply baked to remove residual solvent. By removing the residual solvent, the interdiffusion of the two layers during the stamping process is minimized. The PDMS stamp with thickness less than 5 mm is prepared from a commercially available PDMS prepolymer (Dow Corning Sylgard 184 base and curing agent) with cross-linker in 10:1 or 12:1 mass ratio. The liquid mixture is stirred for 15 min until it

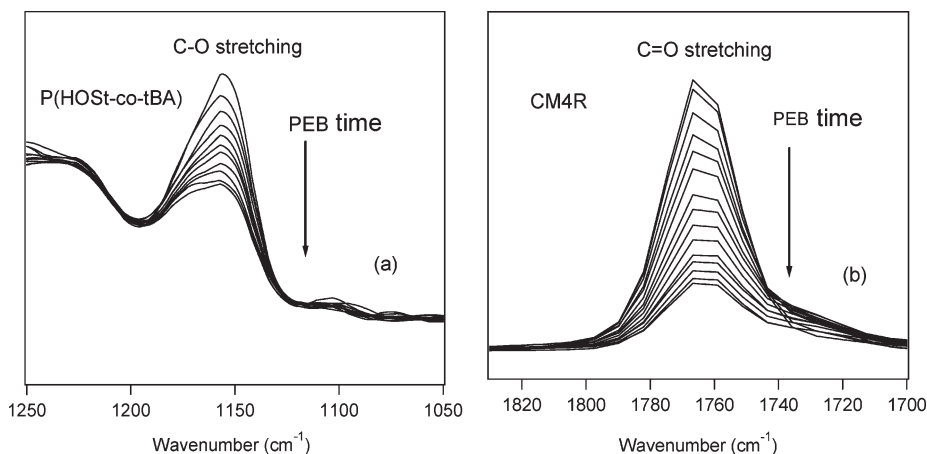


Figure 3. (a) C–O stretching vibrational band evolution during PEB for P(HOST-co-tBA). (b) C=O stretching vibrational band evolution during PEB for CM4R.

becomes opaque and then poured onto a separate clean silicon wafer that rests inside a larger dish. Typically a 5 mm thick stamp works well and has sufficient mechanical properties. This entire dish is placed into a vacuum chamber to remove air bubbles, after which the PDMS is cured in a preheated oven at 70 °C for 1 h. The PDMS stamp is then cooled to room temperature. A circular piece is cut using a razor blade and peeled off from the silicon wafer. This smooth surface that was in contact with the wafer is the top of the stamp. In order to improve the wetting properties for spin-coating the resist solutions on the PDMS stamp, the PDMS surface is treated with oxygen plasma for 5 s at an oxygen flow rate of 2 scfh. The stamp can then be placed onto a spin-coater to prepare the top layer film (nominally 80 nm to 300 nm thick) without a subsequent bake. Finally, the film is transferred from the PDMS substrate to the bottom layer by gently resting the film side down onto the bottom layer film, making contact between the two polymer films. Wait until the PDMS has completely established contact with the bottom layer film, typically about 10 min. Transfer the sample stack to a hot plate preheated to 90 °C, gently compress the PDMS stamp for about 20 s, and then move the sample to a benchtop to cool. Slowly peel off the PDMS stamp. The film should have transferred from the PDMS, making a bilayer. This bilayer stack is then PAB for 60 s at the same PAB temperature used for the bottom layer to remove residual solvent in the top layer.

2.3. Fourier Transform Infrared Reflectance Absorption Spectroscopy. The C–O ($\nu_{C-O} \approx 1160 \text{ cm}^{-1}$) stretch vibrational spectroscopic band is used to quantify the deprotection level of P(HOST-co-tBA) upon PEB (Figure 3a), while the C=O stretch ($\nu_{C=O} \approx 1760 \text{ cm}^{-1}$) is used for CM4R (Figure 3b). All FTIR spectra were collected with a Bomem FTLA 2000 instrument in reflection mode at 16 cm^{-1} resolution. Silicon wafers were coated with Au to increase IR reflectivity and mounted on a preheated hot stage though vacuum contact for the PEB studies. Film thicknesses were measured separately with a J.A. Woollam IR variable angle spectroscopic ellipsometer with an uncertainty of 1–2 nm estimated by one standard deviation based on a calibration with film thickness determined by X-ray reflectivity.

2.4. Reaction–Diffusion Kinetics Model. The details of the modeling approach are discussed elsewhere,^{21,55} and in the Supporting Information only a brief summary is presented. In general, there are three main parts; the first uses Dill's equation to describe the photoacid generation process in eq 1.

$$H = [\text{PAG}](1 - e^{-CE}) \quad (1)$$

$$\frac{d\phi}{dt} = k_P H(1 - \phi) \quad (2)$$

$$\frac{\partial H}{\partial t} = D_H \nabla^2 H - k_T H \phi \quad (3)$$

where [PAG] is the initial photoacid generator loading and H is concentration of photoacid after exposure to a UV exposure dose (E). The Dill constant, C , parametrizes the type of PAG, efficiency, and UV wavelength dependence. In this study, we apply to the sample a 248 nm broad-band UV dose (Oriental Corporation) that is high enough (150 mJ/cm^2) so that all the PAG are activated according to the Dill constant obtained previously.²¹ In this case, the initial acid concentration H_0 is simply equal to the PAG concentration. Equation 2 describes the deprotection reaction such that the rate of change in deprotection level (ϕ) is determined by a first-order reaction between resist protected species ($1 - \phi$) and photoacid concentration with reaction rate constant (k_P).

Equation 3 describes the transport properties of photoacid. A Fickian diffusive term is used to model the center-of-mass photoacid diffusion where D_H is the diffusion constant. While the photoacid diffuses as an electrolyte composed of proton (H^+) and counteranion, we simplify this by an effective diffusion constant. The second term is a process that describes a stoichiometric loss of photoacid. The photoacid trapping mechanism with acid trapping rate constant k_T was introduced in our previous work^{21,55–57} with the notion that photoacids may be kinetically trapped by the reaction products. In a previous study, we demonstrated that deprotection domains are formed in partially reacted photoresist films. This heterogeneous structure is formed by the reaction–diffusion of individual photoacids and the subsequent hydrogen-bonding aggregation.⁵⁵ The strong hydrogen-bonding interactions between the photoacid and the pendant polar groups act as a trap. The trapping rate depends first order on the local deprotection level (ϕ) such that a higher deprotection level induces a larger trapping rate.

2.5. Kinetics Parameters Preliminaries. FTIR measures the time evolution of the average deprotection level of the film. For single layer films, the average deprotection level applies to the whole film assuming the reaction is uniform. For bilayer films, the deprotection level in the top versus bottom layer will be different as suggested by step 4 in the schematic of Figure 2 because the photoacid generator is initially only in the top layer. Since each layer undergoes different extents of reaction due to photoacid diffusion, the measured average deprotection level will depend on the relative film thicknesses of the bilayer film. Therefore, the data must be normalized to determine how much additional reaction takes place between single layer and bilayer experiments.

A relative deprotection level was defined as the average deprotection level normalized to the thickness of acid feeding layer. If there is no acid diffusion, the relative deprotection level of bilayers is equal to the average deprotection level for the single layer. In the presence of photoacid diffusion, the relative deprotection of bilayers is always larger than the single layer film counterpart with the same PAG loading, exposure dose, and

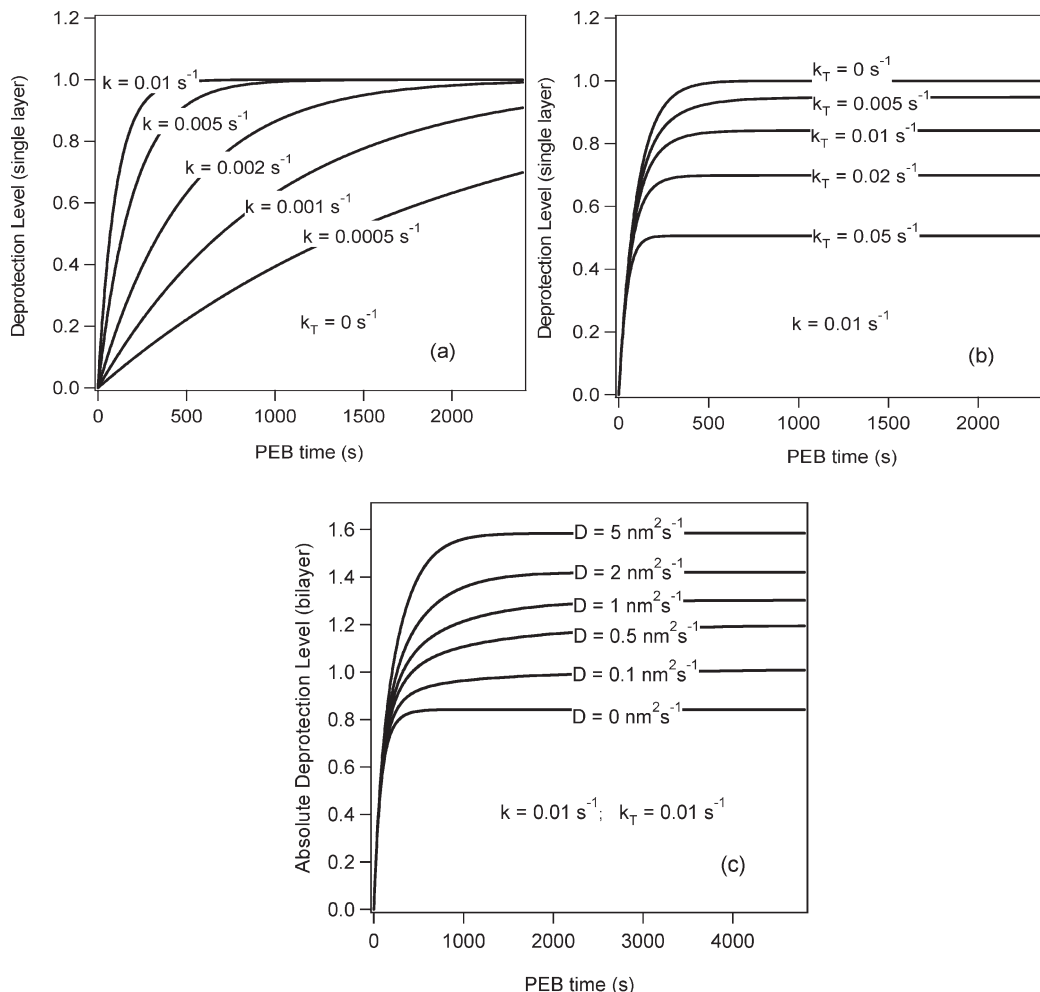


Figure 4. Simulated results: (a) deprotection level vs PEB time at different reaction rate k ($k_T = 0$ is fixed) for single layer film; (b) deprotection level vs PEB time at different trapping rate k_T ($k = 0.01$ s⁻¹ is fixed) for single layer film; (c) absolute deprotection level vs PEB time at different diffusion coefficient D_H ($k = 0.01$ s⁻¹ and $k_T = 0.01$ s⁻¹ are fixed) for bilayer film (thickness for acid feeding layer and the acid-free layer used in the simulation are 50 and 100 nm, respectively). When $D_H = 0$, the curve is the same as in single layer case.

PEB conditions. Therefore, it is expected that the relative deprotection to that of the single layer is greater than 1 for bilayer films although the average deprotection level is always less than 1. The three kinetic parameters are determined by simultaneously fitting the zero-gradient (single layer) and one-dimensional gradient (bilayer) reaction kinetics with the above model. Subsequently, with known initial conditions and three fit parameters the deprotection profile $\phi(z)$ may be calculated for any PEB time.

The uniqueness of the kinetics parameter measurements and how they influence the shapes of the reaction kinetics curves are illustrated by the following examples. At the early stage of the deprotection reaction, the deprotection level for a single layer film approximately follows an exponential rate law due to the insignificance of the trapping term $k_T H \phi$ at small deprotection level. This exponential increase of deprotection is dictated primarily by the reaction rate constant, $k = k_P H_0$, with the known initial photoacid concentration, H_0 . At the later stage of the deprotection reaction, most of the photoacid becomes inactive due to trapping process and the deprotection level plateaus. For a single layer film, it was demonstrated that this plateau level depends on the ratio of trapping constant k_T to reaction rate constant, k_P , $r = k_T/k_P$.²¹ Thus, two of the three parameters are uniquely determined and estimated by the asymptotic curve features from the early and late stage of deprotection. The third parameter, diffusion coefficient D_H , cannot be determined by the proposed mean-field reaction kinetics modeling of single layer reactions because there is no

gradient of the acid concentration. According to eq 3, D_H does not appear in the final function of deprotection level. However, D_H will determine the plateau level of the relative deprotection for the bilayer samples jointly with the other two parameters predetermined from single layer results. Thus, these three parameters can be uniquely determined by fitting the single layer and bilayer kinetics data simultaneously.

Figure 4 shows the sensitivity of the expected deprotection level as a function of reaction time for single layer (a, b) and bilayer (c) reaction kinetics. In the absence of any acid loss mechanisms ($k_T = 0$ s⁻¹) and increasing reaction rate constant the deprotection always goes to completion, as shown in Figure 4a for a single layer. Figure 4b demonstrates the plateau level in deprotection extent by varying the trapping constant over experimentally obtainable scales $k_T = 0$ – 0.05 s⁻¹ with k_P fixed at 0.01 s⁻¹. For the bilayer case for fixed trapping and reaction constants there is sensitivity to the effective diffusion constant simply from the plateau in average deprotection.

3. Results and Discussion

3.1. Acquisition of Kinetics Parameters. *3.1.1. Reaction Rate and Photoacid Trapping Constants: Single Layer Gradient-Free Approach.* The deprotection changes with PEB time were measured by FTIR as a function of temperature for single layer films of P(HOST-co-tBA) and CM4R (Figure 5a,b). It can be seen that the deprotection level has a fast increase at the early

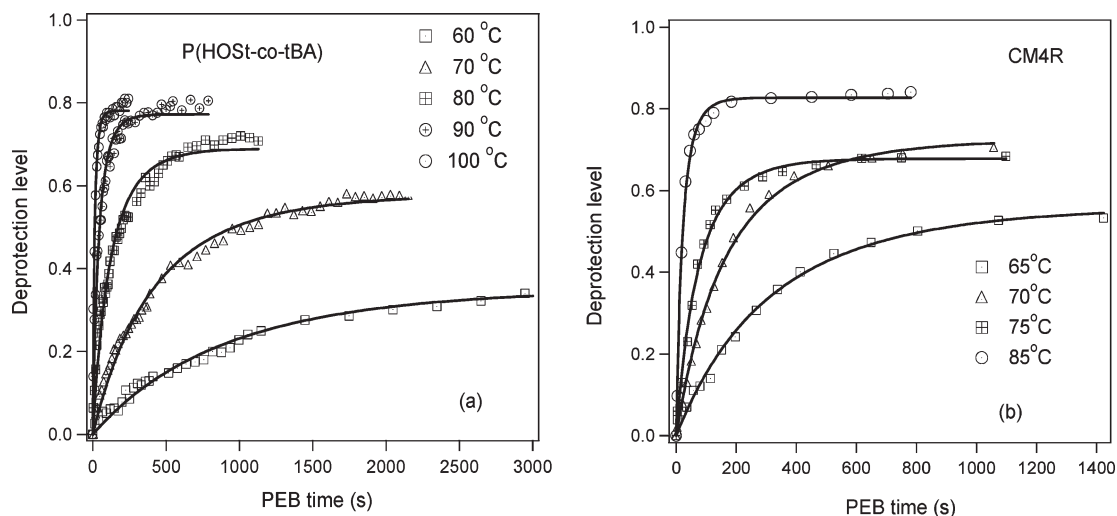


Figure 5. Average deprotection level change in single layers with PEB time and temperature: (a) P(HOST-*co*-tBA) with 2% PAG loading; (b) CM4R with 1% PAG loading. Uncertainty in the deprotection quantification is $\approx(0.01-0.02)$. The solid lines are the fitted curves from the kinetics model.

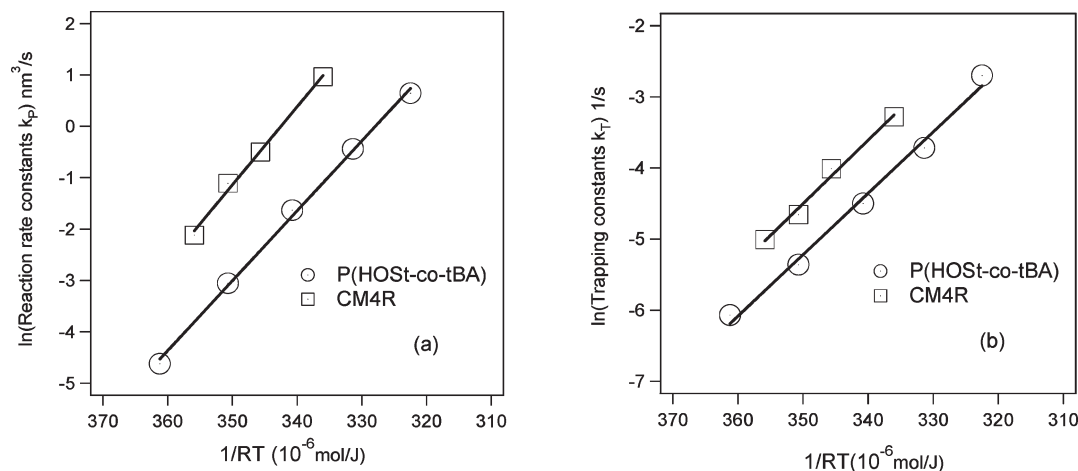


Figure 6. Reaction rate constants (a) and photoacid trapping constant (b) for P(HOST-*co*-tBA) and CM4R at various PEB temperature. The solid lines are Arrhenius model fits.

stage of the PEB time and saturates below completion (deprotection of 1.0) at the later stage for a given PEB temperature. The increased rate and the saturation level of deprotection level are governed by the reaction rate constants and trapping constants (see Figure 4). The lines are fits to the model in the absence of diffusivity ($D=0$), and the results for the temperature dependence of the reaction constants are shown in Figure 6 for both P(HOST-*co*-tBA) and CM4R. For Figure 5, P(HOST-*co*-tBA): $\gamma = 0.02$, $\rho = 1.2 \text{ g/cm}^3$, $H_0 = 0.0257 \text{ nm}^{-3}$; CM4R: $\gamma = 0.01$, $\rho = 1.2 \text{ g/cm}^3$, $H_0 = 0.0129 \text{ nm}^{-3}$. PAG loading and the initial acid concentration can be converted from the formula $[\text{PAG}]_0 = H_0 = \gamma\rho N_A/M_{\text{PAG}}$, where γ is the mass fraction of PAG in resist film, ρ is the mass density of polymer resists, M_{PAG} is the molecular mass of PAG, and N_A is Avogadro's constant.

The reaction and trapping rate constants follow an Arrhenius dependence with fits to $\ln k_P = A - E_a/RT$ with activation energy (E_a) and collision prefactor (A). Figure 6 shows that both k_P and k_T are larger for CM4R than P(HOST-*co*-tBA) at equal PEB temperatures. The activation energy and prefactor for reaction in CM4R are also slightly larger than the P(HOST-*co*-tBA) and shown in Table 1.

3.1.2. Photoacid Diffusion Coefficient: Bilayer, One-Dimensional Gradient, Approach. As mentioned in section 2.4,

Table 1. Arrhenius Parameters for Photoacid Reaction and Acid Trapping

	reaction rate constant		photoacid trapping constant (s^{-1})	
	A	E_a (kJ/mol)	A	E_a (kJ/mol)
P(HOST- <i>co</i> -tBA) ^a	45 ± 1	136 ± 3	25 ± 2	86 ± 5
CM4R ^a	52 ± 3	152 ± 8	27 ± 2	89 ± 7
PBOCSt ²⁰	42	120		

^aUncertainties shown are one standard deviation from the mean of three measurements.

by experimentally introducing a well-defined step photoacid gradient there is explicit spatial sensitivity to measure the photoacid diffusion coefficient due to the additional reaction when compared to the single layer (no gradient). By simultaneously fitting the FTIR reaction kinetics data to both single layer and bilayer films, the three kinetics parameters k_P , k_T , and D_H can be extracted in the same fit as shown in Figure 7. It can be seen that the basic reaction-diffusion kinetics model fits both the single layer and bilayer films with one set of parameters. The introduction of a one-dimensional gradient allows the extra deprotection as shown by the higher relative deprotection extent for the bilayer. The results of the reaction-diffusion kinetics parameters in P(HOST-*co*-tBA)

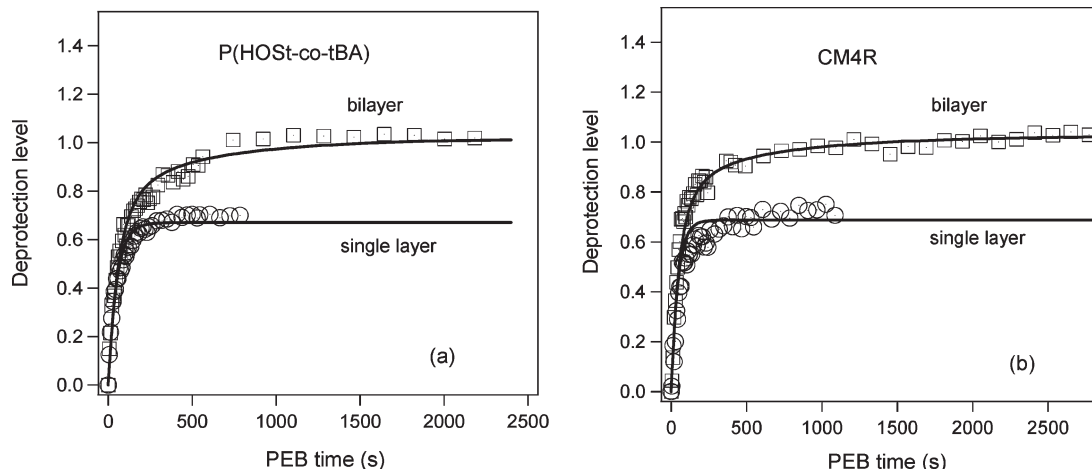


Figure 7. Relative deprotection level vs PEB time for single layer and bilayer in P(HOST-co-tBA) film samples at temperature 90 °C (a) and in CM4R film samples at temperature 70 °C (b). The initial PAG loading for top layer of the bilayer and the single layer are 2 and 5 mass % for (a) and (b), respectively. Exposure dose $\approx 150 \text{ mJ/cm}^2$. The solid lines are fitted curves with kinetics model.

Table 2. Reaction–Diffusion Parameters for P(HOST-co-tBA)^a

	top/bottom layer (nm)	$k_P (\text{nm}^3 \text{s}^{-1})$	$k_T (\text{s}^{-1})$	$D_H (\text{nm}^2/\text{s})$
thin film; 2% PAG	64.8/89.1	0.48	0.0267	4.5
thick film; 2% PAG	69.0/211.2	0.47	0.0279	4.1
thick film; 5% PAG	71.1/222.3	0.58	0.0304	3.9
average ^b		0.51 ± 0.06	0.028 ± 0.002	4.2 ± 0.3

^a PEB temperature of 90 °C. The single layer film is also prepared through PDMS film transfer technique onto Si wafer. ^b Average of three values with uncertainty given as one standard deviation.

at 90 °C PEB are listed in Table 2 for three different samples. It can be seen that the reaction constants and photoacid diffusion constant are independent of bilayer thickness and initial PAG concentration by comparing 2 and 5 mass % TPS-PFBS. This highlights that the PDMS stamping approach is reproducible and leads to self-consistent experimental results.

The temperature dependence of the diffusion coefficients measured for P(HOST-co-tBA) and CM4R is shown in Figure 8. The Arrhenius prefactor and activation energy from fitting $\ln D$ vs $1/RT$ are listed in Table 3. Similar to the reaction constants in Figure 5, the photoacid diffusion constants in Figure 8 show that the same PFBS photoacid has a larger diffusion coefficient in CM4R than in P(HOST-co-tBA) at the same PEB temperature. Table 3 summarizes that CM4R has similar prefactor and activation energy, within experimental uncertainty, as those of poly(*tert*-butoxycarbonyloxystyrene) (PBOCSt). The PBOCSt from the Houle study and CM4R in this study have the same tBOC protection groups.

The FTIR approach provides a simple methodology to estimate photoacid diffusion coefficients. A direct method is to measure the deprotection profile by neutron reflectivity.³⁴ Our previous study³³ with deuterium-labeled P(HOST-co-tBA) shows that the photoacid diffusion constant is $\approx 1.3 \text{ nm}^2/\text{s}$ at 90 °C PEB, which is in good agreement with the current measurements ($4.2 \text{ nm}^2/\text{s}$) under similar experimental conditions. A major difference is that in the neutron reflectivity study the photoacid feeder layer was not the same resist polymer, and the photoacid bilayer system was reversed. The PAG feeder layer could impose a different initial acid transport rate. The soft-lithography stamping method described here provides one diffusion media and therefore eliminates such ambiguity.

3.2. Reaction Kinetics Parameters. **3.2.1. Diffusion Coefficients.** The measurements and model show that the photoacid

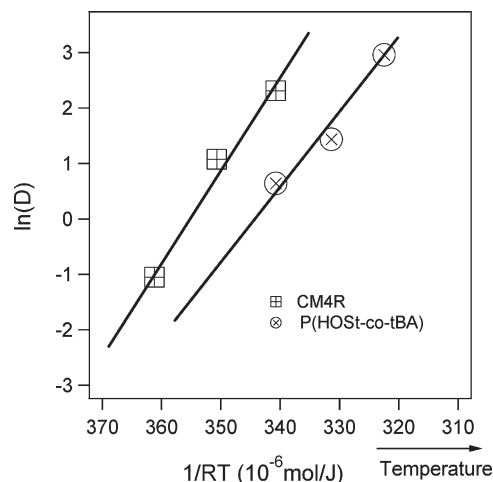


Figure 8. Natural logarithm of measured photoacid diffusion coefficients for CM4R and P(HOST-co-tBA) versus inverse PEB temperature. The solid lines are fits to the Arrhenius equation.

Table 3. Activation Energy of Photoacid Diffusion Coefficients

$D_H = A \exp(-E_a/RT)$	$A (\text{nm}^2/\text{s})$	$E_a (\text{kJ/mol})$
P(HOST-co-tBA)	44 ± 8	127 ± 25
CM4R	59 ± 8	165 ± 23
PBOCSt ²⁰	51	153

diffusion coefficients and reaction constants are systemically larger in CM4R than P(HOST-co-tBA) at the same temperature. The PEB conditions we employ are below the calorimetric glass transition of the resist for tBOC-protected CM4R and P(HOST-co-tBA); the T_g s are 107 °C [ref 58] and 150 °C [ref 59], respectively. Even though the processing temperature is closer to T_g with the molecular glass, below T_g the glassy dynamics

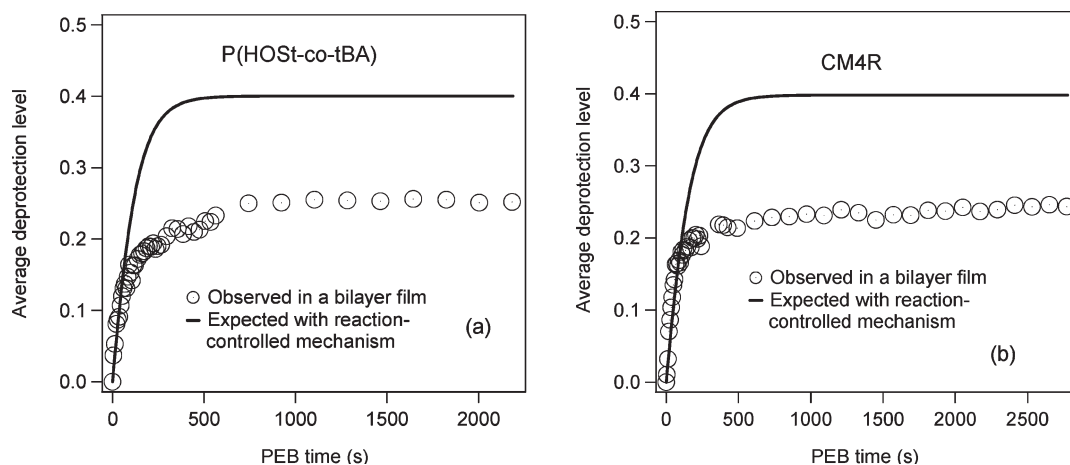


Figure 9. Average deprotection level vs PEB time for bilayer in P(HOST-co-tBA) film samples at temperature 90 °C (a) and in CM4R film samples at temperature 70 °C (b). The dots are the measured data; the solid lines are the calculated by assuming the deprotection is reaction-controlled in which the reaction rate constant and trapping constant are the same as those in the corresponding single layer film.

strictly do not depend upon the glass transition temperature, since the temperature dependence lacks a reference temperature. This is supported by the observations that the kinetics and diffusion constants follow an Arrhenius dependence that lacks a reference temperature, such as T_g . Well above T_g , however, the temperature dependence of the dynamics should follow a Vogel–Fulcher (equivalent to Williams–Landel–Ferry) dependence that requires a reference temperature ($T - T_g$).⁶⁰ It is interesting to note that most polymer resists display an increase in T_g with deprotection owing to the strong interactions of the polar groups, whereas the calix[4]resorcinarene molecular glass studied here undergoes a decrease in T_g with deprotection; the T_g of the fully protected CM4R is 107 °C, while that of the unprotected CM4R is 84 °C [ref 58]. So, it appears that the effect of protection level on T_g is not general with photoresists.

We attribute the larger diffusivity of the same photoacid in the molecular glass than polymer as strongly influenced by the hydrogen-bonding interaction. The photoacid is a strong hydrogen-bond donor, while the phenol on PHOST and/or the carbonyl are hydrogen-bond acceptors with the P(HOST-co-tBA). In CM4R the C=O is mostly shielded by the tBOC protection groups and not easily accessible and do not hydrogen bond. This difference in interaction may partly explain the larger diffusivity in CM4R. However, as the deprotection reaction occurs, these specific interactions between photoacid and newly formed deprotected polar groups, hydroxyls in CM4R and acrylic acid in P(HOST-co-tBA), strongly influence the photoacid transport. The interaction with these polar groups was demonstrated in a model systems.^{61,62} The local deprotection structure may additionally slow down the photoacid and effectively trap them. This would be reflected by the higher trapping rate (shorter photoacid lifetime) that reduces the overall photoacid diffusion length in CM4R.

3.2.2. Reaction Rate Constants. The reaction–diffusion of photoacid in chemically amplified resists is generally believed to be diffusion-controlled. This can be demonstrated by analyzing the experimental data for single layer and bilayer films. Parts a and b of Figure 9 show a comparison of the average deprotection level of bilayer film sample for P(HOST-co-tBA) and CM4R, respectively, as a function of PEB time between the measured and the expected result under a hypothetical reaction-control mechanism. In a reaction-controlled situation, the photoacid diffuses very fast, and the concentration of photoacid quickly reaches an equilibrium state in the whole bilayer film beginning with

the top layer or the acid feeding layer. However, it can be seen that the measured average deprotection level for bilayer film (the real situation) is far lower than that expected in the reaction-controlled condition. This suggests that the concentration of photoacid does not disperse uniformly in the bilayer film, but rather forms a gradient. Therefore, the deprotection reaction is diffusion-controlled and more consistent with our observations.

A diffusion-controlled photoacid-catalyzed reaction can be described by a random walk model where the photoacid hops from site-to-site within the glassy matrix. If the reaction is treated as an effective collision between two molecules (Smoluchowski rate), the reaction rate constant or can be related to the diffusion coefficient by⁶³

$$k_p = 4\pi\alpha(D_1 + D_2)(r_1 + r_2) \quad (4)$$

where the α is the reaction probability per collision, the D_1 and D_2 are the diffusion coefficient for the two molecules, and the r_1 and r_2 are the molecular radii. Considering the collision is not between two free molecules but between a free molecule or the proton and a functional group in a quasi-static matrix, eq 4 can be rewritten to be as the following if all the functional groups (more accurately the reaction site) are in a cubic lattice.⁶⁴

$$k_p = 6\alpha DL \quad (5)$$

where L is the step length in the cubic lattice model and α the probability of the acid-labile reaction per collision. If α and L do not differ much for CM4R or P(HOST-co-tBA), eq 5 suggests that the reaction rate constant increases with diffusion coefficient. This is consistent with the two resists studied. α is the local reaction rate in which the transport factor can be ignored; therefore, it can be best measured when the acid-catalyzed reaction occurs in solution state. We do not have this information yet. However, Wallraff found that the reaction rate constant for the acid-catalyzed reaction with TPS-PFBS is greater in PBOCSt than in poly(*tert*-butyl acrylate), PTBA.⁶⁵ These resist systems differ by the acid-labile protecting group which suggests the reaction probability for *tert*-butylcarbonate (tBOC) is larger than *tert*-butyl (tB). In other words, the acid-labile reaction is easier in a resist with tBOC than that with tB. This could be an additional factor to account for the larger reaction rate in MG.

It is interesting to note that with the measured reaction rate constants and the diffusion coefficient the reaction

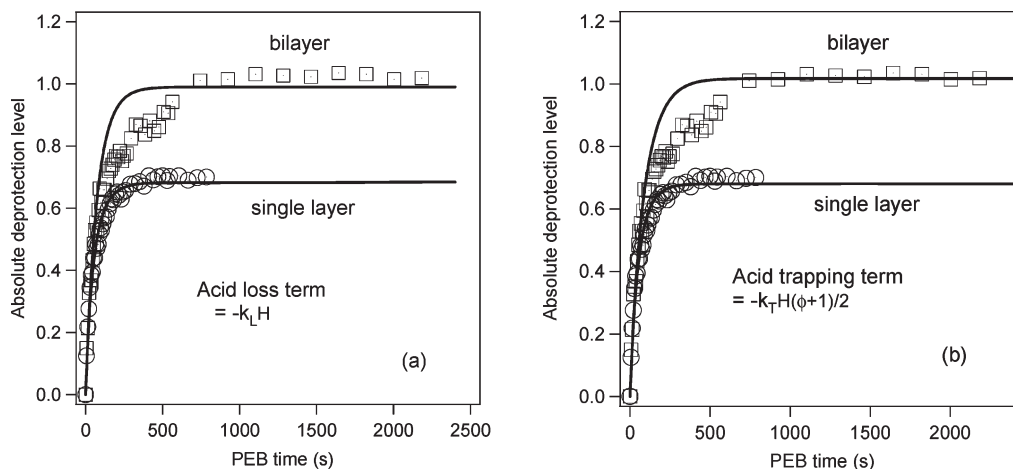


Figure 10. Deprotection level vs PEB time for single layer and bilayer in P(HOST-*co*-tBA) film samples at temperature 90 °C. The solid lines are fitted curves with kinetics model with acid loss term (a) $-k_L H$ and (b) $-k_T H(\phi + 1)/2$. Both model fit the single layer data very well but the bilayer data poorly. The diffusion coefficient to the bilayer experiments are found to be $> 350 \text{ nm}^2/\text{s}$ (a) and $45 \text{ nm}^2/\text{s}$ (b) with best fit.

probability can be estimated to be around 0.03 and 0.05 for P(HOST-*co*-tBA) and MG, respectively (L is assumed to be 0.5 nm). These numbers imply that one reaction occurs every 33 collisions and 20 collisions for the polymer and molecular resist, respectively. Measurements that are able to probe the local dynamics of these reaction at nanometer length scales would be an interesting test of these predictions.

The activation energy for reaction rate constants is not far away from that of the diffusion coefficients from Tables 2 and 3. This is another evidence about that the acid-catalyzed reaction is dominated by diffusion. Consequently, the activation energy of α , the local reaction rate, is very low. This fact suggests that the acid-labile reaction is more like the ion-initiated reaction instead of free-radical-initiated which usually has a larger activation energy barrier.⁶⁶

3.2.3. Phenomenology of the Trapping Constants. The diffusion of photoacids is generally non-Fickian.³⁶ This can be evident from the fact that the reaction actually stops at deprotection levels less than 1, particularly for single layer films, indicating that the photoacid has become inactive or been lost. Because of the non-Fickian behavior, various models have been proposed to describe this phenomenon. Houle et al.^{20,65} suggest an equilibrium state for the acidic protons to reside on protected and deprotected moieties; therefore, there are always some protons that are no longer active for deprotection because they reside in deprotected products. This implies that the photoacid is not active at all times but may appear lost or dormant due to local equilibration. Other approaches include an acid loss term in the Fickian diffusion equation. In most cases^{36,67} the acid loss term is modeled as $-k_L H$, where k_L is called acid loss constant, suggesting that the acid loss rate is first order in acid concentration and independent of the deprotection level.

In our study, we model the acid loss as $-k_T H\phi$ to incorporate the influence of the deprotection reaction.²¹ There is almost no difference in describing the single layer film system between these two models except that the k_T is usually larger than k_L because the deprotection level is always less than one. However, it is necessary to use the trapping mechanism of eq 3 with first-order dependence on the deprotection extent to describe the deprotection profile at the interface of a bilayer system.¹⁷ Figure 10a shows the results of curve fitting for the bilayer kinetics data using the literature acid loss model. We assume that the same set of parameters is applicable for both single layer and bilayer films just as we did with our current model. We found that

fitting to the data is poor, particularly around the PEB time period before the reaction reaches saturation. Moreover, the diffusion coefficient obtained with this model is unreasonably high when compared previous neutron reflectivity results.³³ These two aspects combined indicate that a trapping mechanism makes more sense in capturing the physical process as shown by Figure 7a.

Another important feature for the trapping mechanism is that trapping is more associated with deprotection domains rather than single moieties. For example, there are 50% HOST groups in P(HOST-*co*-tBA), but since P(HOST-*co*-tBA) is a random copolymer, the HOST groups are uniformly distributed in the resist. However, local hydrophilic domains form during the deprotection reaction due to the discrete nature of the photoacid and the local aggregation;⁵⁶ the photoacid could be effectively slowed down and even stopped by these domains until all the photoacid become inactive. Hence, this is referred to as a phenomenological trapping process. This point will be illustrated with Figure 10b as follows. If the photoacid is trapped by every polar functional group, the stoichiometry of the trapping term for P(HOST-*co*-tBA) should be $-(0.5k_T H\phi + 0.5k_T' H)$. Since both the HOST and the MAA are strongly polar groups, we can assume $k_T = k_T'$. Such a kinetics model can fit the single layer data very well, but we encounter the same problem as the acid loss model of Figure 10a when fitting the bilayer data. This implies that trapping does not occur with a single molecule or moiety rather with a polar domain.

In our previous study, we demonstrated that deprotection domains are formed in partially reacted photoresist films. This heterogeneous structure is formed by the reaction-diffusion of individual photoacids and the subsequent hydrogen-bonding aggregation.⁵⁵ The degree of heterogeneity was quantified, as an order parameter, based upon the relative fraction of hydrogen-bonded versus free carboxylic acid groups. The scaling of the degree of heterogeneity with deprotection extent as well as copolymer content verified the hypothesis of localized domains with nonrandom distribution. Further, the heterogeneity reaches a maximum at intermediate deprotection extents that serves as kinetic traps of the diffusing photoacids. In the present case, since CM4R has a relatively lower T_g , it may be easier for dynamically rearranging regions to form a heterogeneous structure with a larger trapping probability.

3.3. Deprotection Profile Predictions and Estimates of the Photoacid Diffusion Length. The photoacid diffusion length can be estimated by developing the bilayer in an aqueous

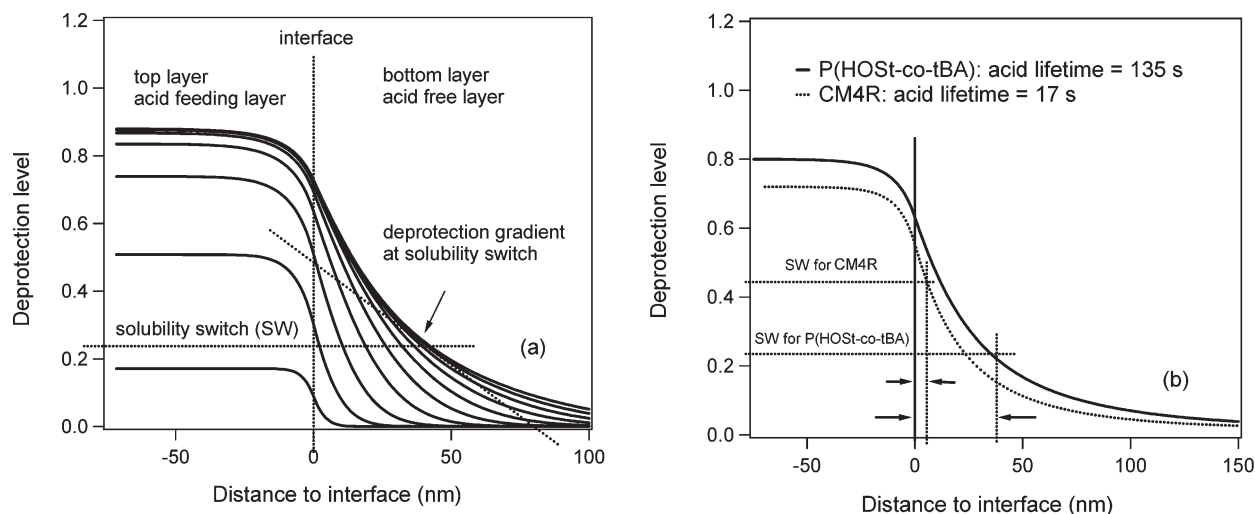


Figure 11. (a) Calculated deprotection profile for P(HOST-co-tBA) at 90 °C PEB temperature for various PEB times. PAG loading in acid feeding layer is 5% by mass fraction. (b) Calculated deprotection profile for P(HOST-co-tBA) and CM4R at 80 °C PEB temperature for 30 min PEB time. PAG loading and dose condition are the same as (a) for both resists.

Table 4. Diffusion Length and Deprotection Gradient for CM4R and P(HOST-co-tBA)

PEB ^{a,b} (°C)	P(HOST-co-tBA)		molecular resist (CM4R)		
	diffusion length (measured/predicted) (nm)	deprotection gradient ^c (nm ⁻¹)	PEB (°C)	diffusion length (measured/predicted) (nm)	deprotection gradient ^c (nm ⁻¹)
80	42/38	0.005	60	4/5	0.022
90	48/45	0.005	70	6/7	0.013
100	(29)/(31)	0.004	80	8/7	0.016

^aThe PAG loading is 5% PAG (or 2% in parentheses) in the acid feeder layer. ^bPEB time = 30 min. ^cThe solubility switch is fitted to be 0.22 for P(HOST-co-tBA) and 0.42 for CM4R.

hydroxide solution as shown in step 5 of Figure 2. The distance between the initial bilayer interface and the developed film thickness is a measure of how far the photoacid diffused and reacted. Experimentally, this length can be determined by subtracting the bottom layer film thickness after PEB and development from its initial thickness. This approach does not require any modeling and permits quantitative comparison among different materials as well as PEB conditions.

This definition of the photoacid diffusion length may also be predicted. Using the reaction and diffusion parameters, the deprotection profiles were calculated to provide the depth profile of deprotection level. Figure 11a shows an example of these deprotection profiles and how they evolve with PEB time for the polymer resist. The diffusion length was estimated by the distance from the initial sharp interface (vertical dotted line) of a bilayer to the intersection between the point of development called the solubility switch (SW) shown as the horizontal line that intersects each profile. Further, the deprotection gradient at the point where development stops (above an average deprotection level) or latent-image log slope (LILS) may be calculated. The LILS is a crucial physical parameter that is correlated to LER and is central to all resolution models.²

The measured and predicted diffusion length and calculated deprotection gradients are listed in Table 4 for several PEB temperatures. First, it can be seen that the measured and calculated diffusion length agree with a single *fitted* solubility switch. This supports the applicability of the kinetics model and parameters used here. For these model conditions of 30 min PEB time, there appears to be a weak dependence on PEB temperature for the diffusion length and deprotection gradient at the same PAG loading. However,

this is due to the fact that the reaction front^{17,68} stops propagating due to the aforementioned photoacid trapping process. One may see by inspection of Figure 11a that the profiles do not propagate unbounded at long times. Under these conditions, even though the initial PAG gradient is sharp, the reaction does not proceed to completely deprotect both layers. Shorter PEB times would show a strong temperature dependence.

The perfluorobutanesulfonate photoacid has a significantly smaller diffusion length in the molecular glass than the polymer resist. Simultaneously, the deprotection gradient at the solubility switch is larger for the molecular glass at the same PEB temperature. The large difference in diffusion length is consistent with the higher deprotection value required to dissolve the molecular glass. The dissolution threshold intercepts the deprotection profile at a shorter distance when compared to the P(HOST-co-tBA), as shown in Figure 11b for a direct comparison. Another reason is that the CM4R has a larger photoacid trapping constant that results in a shorter acid lifetime even though the diffusion coefficient and reaction rate constant are larger. Therefore, it is the combination of reaction–diffusion parameters (k_p , k_T , and D_H) and position of the solubility switch that determines the photoacid diffusion length.

As a consequence and importance of all three parameters, a conversion of the diffusion constant to a diffusion length using $l_d = (2Dt)^{1/2}$ differs from the diffusion length (L_d) defined as the change in thickness after development of the bilayer. The L_d is not proportional to $t^{1/2}$ at all times, contrary to what is generally believed. With the measured kinetic parameters, the diffusion length was *calculated* as a function of PEB time for various PEB temperatures for P(HOST-co-tBA), as shown in Figure 12. Initially, the L_d

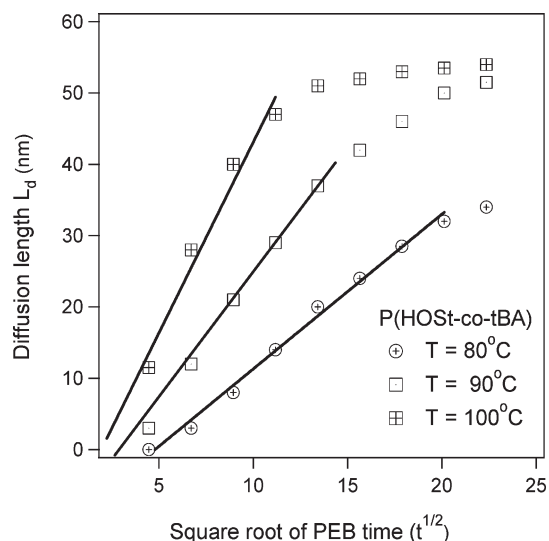


Figure 12. Simulated diffusion length L_d for P(HOSSt-co-tBA) at various PEB temperatures.

appears to follow a $t^{1/2}$ diffusive scaling; however, a systematic deviation occurs and eventually a plateau in L_d . In addition, each line is offset which indicates that L_d is not only proportional to $t^{1/2}$. The early and intermediate time behavior is consistent with the experiments of Goldfarb et al.⁶⁹ Thus, using $l_d = (2Dt)^{1/2}$ to estimate diffusion length from known diffusion coefficient or to estimate the diffusion coefficient from measured diffusion length is only valid for Fickian diffusion or in the absence of photoacid loss or trapping processes.

The experimental methods discussed should be of more general use to fabricate test structures with high fidelity in other research areas as well as extendable to other wavelength exposures. Experiments to provide even more stringent tests of the deprotection profiles using neutron reflectivity are in progress. When compared to more sophisticated analysis methods, it is clear that a rapid experimental method is needed to test aspects of photoacid diffusion and critical additives used to counteract the effects of image blur. In the context of these experiments the soft-lithography methods described here have proven useful to compare commercial and model materials.

Of general interest to photoresists and other polymer science problems is transport below, near, and above the glass transition. Our observations of Arrhenius dependence is consistent with the literature for activated transport below the calorimetric glass transition.⁶⁰ However, even one-component glasses exhibit a dynamic heterogeneity. The local motions of molecules exhibit dynamically rearranging regions of widely varying domain size and relaxation times.^{60,70,71} However, difficult photoresist problems are more closely related to multicomponent copolymer glasses.^{72–75} The experimental methods developed could be used to extend the multilayer strategies to study transport and dynamic heterogeneity in a wider variety of multicomponent systems.^{75–78} Since our observations of photoacid trapping requires a static chemical heterogeneity formed by the reaction, it would be interesting to discuss the photoacid transport in the context of dynamic heterogeneity.

4. Conclusions

A methodology to determine photoacid diffusion coefficients was developed using a specially prepared bilayer films to create a sharp step function profile of PAG distribution. While this model

lithographic line edge has been created experimentally before, this work presents the first demonstration of photoacid diffusion across the same diffusion medium with a sharp initial PAG distribution. The sharp interface mimics an ideal step exposure line edge but also is applicable to base quencher additives and extendable to any other chemically amplified resist systems. With this new developed methodology, we have characterized and compared the kinetics of two model EUV photoresists: a molecular glass and a polymeric resist. We found that the reaction rate constant, trapping constant, and the diffusion constant are all larger in the molecular glass at equal PEB temperature. In addition, the diffusion length and reaction–diffusion front do not simply depend on an effective photoacid diffusion coefficient; they dependent also on the photoacid trapping rate which reduces the lifetime of the photoacid.

Acknowledgment. This work was supported by a cooperative research and development agreement between Intel Corp. and NIST (CRADA 1893). We also acknowledge Manish Chandhok, Wang Yueh, Todd Younkun, Melissa Shell, Michael Leeson, George Thompson, and Christof Krautschik from Intel and Eric Lin and Christopher Soles from NIST for their support. The Cornell authors thank the Semiconductor Research Corporation for funding. The Cornell Nanoscale Science and Technology Facility and the Cornell Center for Materials Research are thanked for use of their facilities. Jim Sounik and Michael Sheehan at DuPont Electronic Materials for synthesizing the polymer used in this study.

Supporting Information Available: Data analysis. This material is available free of charge via the Internet at <http://pubs.acs.org>.

References and Notes

- Hinsberg, W.; Houle, F. A.; Hoffnagle, J.; Sanchez, M.; Wallraff, G.; Morrison, M.; Frank, S. *J. Vac. Sci. Technol. B* **1998**, *16* (6), 3689–3694.
- Pawloski, A.; Acheta, A.; Lalovic, I.; LaFontaine, B.; Levinson, H. *Proc. SPIE* **2004**, *5376*, 414.
- Ito, H. *Adv. Polym. Sci.* **2005**, *172*, 37–245.
- Ito, H. *J. Polym. Sci., Part A: Polym. Chem.* **2003**, *41* (24), 3863–3870.
- Willson, C.; Ito, H.; Frechet, J.; Tessier, T.; Houlihan, F. *J. Electrochem. Soc.* **1986**, *133*, 181–187.
- Houle, F. A.; Hinsberg, W. D.; Sanchez, M. I.; Hoffnagle, J. A. *J. Vac. Sci. Technol. B* **2002**, *20* (3), 924–931.
- Wallraff, G. M.; Hinsberg, W. D. *Chem. Rev.* **1999**, *99* (7), 1801–1821.
- Kim, J. H.; Kim, Y. H.; Chon, S. M.; Nagai, T.; Noda, M.; Yamaguchi, Y.; Makita, Y.; Nemoto, H. *J. Photopolym. Sci. Technol.* **2004**, *17* (3), 379–384.
- Schmid, G. M.; Stewart, M. D.; Singh, V. K.; Willson, C. G. *J. Vac. Sci. Technol. B* **2002**, *20* (1), 185–190.
- Stewart, M. D.; Tran, H. V.; Schmid, G. M.; Stachowiak, T. B.; Becker, D. J.; Willson, C. G. *J. Vac. Sci. Technol. B* **2002**, *20* (6), 2946–2952.
- Hoffnagle, J. A.; Hinsberg, W. D.; Sanchez, M. I.; Houle, F. A. *Opt. Lett.* **2002**, *27* (20), 1776–1778.
- International Technology Roadmap for Semiconductors, **2004** Update; 04.
- Shi, X. L. *J. Vac. Sci. Technol. B* **1999**, *17* (2), 350–354.
- Itani, T.; Yoshino, H.; Fujimoto, M.; Kasama, K. *J. Vac. Sci. Technol. B* **1995**, *13* (6), 3026–3029.
- Croffie, E.; Yuan, L.; Cheng, M. S.; Neureuther, A.; Houlihan, F.; Cirelli, R.; Watson, P.; Nalamasu, O.; Gabor, A. *J. Vac. Sci. Technol. B* **2000**, *18* (6), 3340–3344.
- Hinsberg, W. D.; Houle, F. A.; Sanchez, M.; Morrison, M.; Wallraff, G. M.; Larson, C.; Hoffnagle, J.; Brock, P.; Breyta, G. *Proc. SPIE, Adv. Resist Technol. Process. XVII* **2000**, 3999, 148.
- Vogt, B. D.; Kang, S.; Prabhu, V. M.; Lin, E. K.; Satija, S. K.; Turnquest, K.; Wu, W. *Macromolecules* **2006**, *39* (24), 8311–8317.

- (18) Goldfarb, D. L.; Angelopoulos, M.; Lin, E. K.; Jones, R. L.; Soles, C. L.; Lenhart, J. L.; Wu, W. L. *J. Vac. Sci. Technol. B* **2001**, *19* (6), 2699–2704.
- (19) Soles, C. L.; Douglas, J. F.; Lin, E. K.; Lenhart, J. L.; Jones, R. L.; Wu, W. L.; Goldfarb, D. L.; Angelopoulos, M. *J. Appl. Phys.* **2003**, *93* (4), 1978–1986.
- (20) Houle, F. A.; Hinsberg, W. D.; Morrison, M.; Sanchez, M. I.; Wallraff, G.; Larson, C.; Hoffnagle, J. *J. Vac. Sci. Technol. B* **2000**, *18* (4), 1874–1885.
- (21) Kang, S.; Prabhu, V. M.; Vogt, B. D.; Lin, E. K.; Wu, W. L.; Turnquest, K. *Polymer* **2006**, *47* (18), 6293–6302.
- (22) Stewart, M. D.; Somervell, M. H.; Tran, H. V.; Postnikov, S. V.; Willson, C. G. *Proc. SPIE* **2000**, *3999*, 665–674.
- (23) Hinsberg, W. D.; Houle, F. A.; Sanchez, M. I.; Wallraff, G. M. *IBM J. Res. Dev.* **2001**, *45* (5), 667–682.
- (24) Hoffnagle, J. A.; Hinsberg, W. D.; Houle, F. A.; Sanchez, M. I. *J. Photopolym. Sci. Technol.* **2003**, *16* (3), 373–379.
- (25) Karim, A.; Mansour, A.; Felcher, G. P.; Russell, T. P. *Phys. Rev. B* **1990**, *42* (10), 6846–6849.
- (26) Karim, A.; Mansour, A.; Felcher, G. P.; Russell, T. P. *Physica B* **1989**, *156*, 430–433.
- (27) Lin, E. K.; Kolb, R.; Satija, S. K.; Wu, W. L. *Macromolecules* **1999**, *32* (11), 3753–3757.
- (28) Lin, E. K.; Wu, W. L.; Satija, S. K. *Macromolecules* **1997**, *30* (23), 7224–7231.
- (29) Kim, S.; Hewlett, S. A.; Roth, C. B.; Torkelson, J. M. *Eur. Phys. J. E* **2009**, *30* (1), 83–92.
- (30) Roth, C. B.; Torkelson, J. M. *Macromolecules* **2007**, *40* (9), 3328–3336.
- (31) Swallen, S. F.; Mapes, M. K.; Kim, Y. S.; McMahon, R. J.; Ediger, M. D.; Satija, S. *J. Chem. Phys.* **2006**, *124*, 18.
- (32) Lee, J. K.; Chatzichristidi, M.; Zakhidov, A. A.; Hwang, H. S.; Schwartz, E. L.; Sha, J.; Taylor, P. G.; Fong, H. H.; DeFranco, J. A.; Murotani, E.; Wong, W. W. H.; Malliaras, G. G.; Ober, C. K. *J. Mater. Chem.* **2009**, *19* (19), 2986–2992.
- (33) Lavery, K. A.; Vogt, B. D.; Prabhu, V. M.; Lin, E. K.; Wu, W. L.; Satija, S. K.; Choi, K. W. *J. Vac. Sci. Technol. B* **2006**, *24* (6), 3044–3047.
- (34) Lin, E. K.; Soles, C. L.; Goldfarb, D. L.; Trinquet, B. C.; Burns, S. D.; Jones, R. L.; Lenhart, J. L.; Angelopoulos, M.; Willson, C. G.; Satija, S. K.; Wu, W. L. *Science* **2002**, *297*, 372–375.
- (35) Vogt, B. D.; Kang, S. H.; Prabhu, V. M.; Rao, A.; Lin, E. K.; Wu, W. L.; Satija, S. K.; Turnquest, K. *J. Vac. Sci. Technol. B* **2007**, *25* (1), 175–182.
- (36) Zuniga, M.; Neureuther, A. *J. Vac. Sci. Technol. B* **1995**, *13* (6), 2957–2962.
- (37) Postnikov, S. V.; Stewart, M. D.; Tran, H. V.; Nierode, M. A.; Medeiros, D. R.; Cao, T.; Byers, J.; Webber, S. E.; Willson, C. G. *J. Vac. Sci. Technol. B* **1999**, *17* (6), 3335–3338.
- (38) Kang, S.; Prabhu, V. M.; Wu, W. L.; Lin, E. K.; Choi, K. W.; Chandhok, M.; Younkin, T. R.; Yueh, W. *Proc. SPIE* **2009**, *7273*, p 72722U-11.
- (39) Karim, A.; Arendt, B. H.; Felcher, G. P.; Russell, T. P. *Thin Solid Films* **1991**, *202* (2), 345–350.
- (40) Ennis, D.; Betz, H.; Ade, H. *J. Polym. Sci., Part B: Polym. Phys.* **2006**, *44* (22), 3234–3244.
- (41) Glodde, M.; Goldfarb, D. L.; Medeiros, D. R.; Wallraff, G. M.; Denbeaux, G. P. *J. Vac. Sci. Technol. B* **2007**, *25* (6), 2496–2503.
- (42) Hirayama, T.; Shiono, D.; Hada, H.; Onodera, J. *J. Photopolym. Sci. Technol.* **2004**, *17* (3), 435–440.
- (43) VanderHart, D. L.; Prabhu, V. M.; De Silva, A.; Felix, N. M.; Ober, C. K. *J. Mater. Chem.* **2009**, *19* (18), 2683–2694.
- (44) Ito, H.; Nakayama, T.; Sherwood, M.; Miller, D.; Ueda, M. *Chem. Mater.* **2008**, *20* (1), 341–356.
- (45) Young-Gil, K.; Kim, J. B.; Fujigaya, T.; Shibasaki, Y.; Ueda, M. *J. Mater. Chem.* **2002**, *12* (1), 53–57.
- (46) Chang, S. W.; Ayothi, R.; Bratton, D.; Yang, D.; Felix, N.; Cao, H. B.; Deng, H.; Ober, C. K. *J. Mater. Chem.* **2006**, *16* (15), 1470–1474.
- (47) Yang, D.; Chang, S. W.; Ober, C. K. *J. Mater. Chem.* **2006**, *16* (18), 1693–1696.
- (48) De Silva, A.; Lee, J. K.; Andre, X.; Felix, N. M.; Cao, H. B.; Deng, H.; Ober, C. K. *Chem. Mater.* **2008**, *20* (4), 1606–1613.
- (49) Felix, N. M.; De Silva, A.; Luk, C. M. Y.; Ober, C. K. *J. Mater. Chem.* **2007**, *17* (43), 4598–4604.
- (50) De Silva, A.; Felix, N.; Sha, J.; Lee, J. K.; Ober, C. K. *Proc. SPIE*, **2008**, *6923*, p 69231L-14.
- (51) De Silva, A.; Felix, N.; Forman, D.; Sha, J.; Ober, C. K. *Proc. SPIE*, **2008**, *6923*, p 69230O-9.
- (52) Choi, K. W.; Prabhu, V. M.; Lavery, K. A.; Lin, E. K.; Wu, W. L.; Woodward, J.; Leeson, M.; Cao, H.; Chandhok, M.; Thompson, G. *Proc. SPIE* **2007**, *6519*, 651943.
- (53) Dai, J. Y.; Chang, S. W.; Hamad, A.; Yang, D.; Felix, N.; Ober, C. K. *Chem. Mater.* **2006**, *18* (15), 3404–3411.
- (54) Lavery, K. A.; Choi, K. W.; Vogt, B. D.; Prabhu, V. M.; Lin, E. K.; Wu, W. L.; Satija, S. K.; Leeson, M.; Cao, H.; Thompson, G.; Deng, H.; Fryer, D. S. *Proc. SPIE* **2006**, *6153*, 615313.
- (55) Kang, S.; Prabhu, V. M.; Vogt, B. D.; Lin, E. K.; Wu, W. L.; Turnquest, K. *Proc. SPIE* **2006**, *6153*, 61533N.
- (56) Kang, S.; Vogt, B. D.; Wu, W. L.; Prabhu, V. M.; VanderHart, D. L.; Rao, A.; Lin, E. K.; Turnquest, K. *Macromolecules* **2007**, *40*, 1497–1503.
- (57) Kang, S.; Vogt, B. D.; Wu, W. L.; Prabhu, V. M.; VanderHart, D. L.; Rao, A.; Lin, E. K.; Turnquest, K. *Proc. SPIE* **2007**, *6159*, 615916.
- (58) Felix, N. M.; De Silva, A.; Ober, C. K. *Adv. Mater.* **2008**, *20* (7), 1303–+.
- (59) Ito, H. *IBM J. Res. Dev.* **1997**, *41* (1–2), 69–80.
- (60) Ediger, M. D. *Annu. Rev. Phys. Chem.* **2000**, *51*, 99–128.
- (61) Lee, J.; Park, K.; Chang, T.; Jung, J. *Macromolecules* **1992**, *25*, 6977–6979.
- (62) Park, H.; Sung, J.; Chang, T. *Macromolecules* **1996**, *29*, 3216–3219.
- (63) Nakamura, J.; Ban, H.; Tanaka, A. *Jpn. J. Appl. Phys.* **1992**, *31*, 4294–4300.
- (64) Kang, S.; Wu, W. L.; Prabhu, V. M.; Vogt, B. D.; Lin, E. K.; Turnquest, K. *Proc. SPIE* **2007**, *6519*, 65193V_1–65193V_10.
- (65) Wallraff, G.; Hutchinson, J.; Hinsberg, W. D.; Houle, F. A.; Seidel, P.; Johnson, R.; Oldham, W. *J. Vac. Sci. Technol. B* **1994**, *12* (6), 3857–3862.
- (66) Stannett, V. T. *Pure Appl. Chem.* **1981**, *53* (3), 673–680.
- (67) Krasnoperova, A. A.; Khan, M.; Rhyner, S.; Taylor, J. W.; Zhu, Y.; Cerrina, F. *J. Vac. Sci. Technol. B* **1994**, *12* (6), 3900–3904.
- (68) Vogt, B. D.; Kang, S.; Prabhu, V. M.; Rao, A.; Lin, E. K.; Satija, S. K.; Turnquest, K.; Wu, W. *Proc. SPIE* **2006**, *6153*, 615316.
- (69) Goldfarb, D. L.; Angelopoulos, M.; Lin, E. K.; Jones, R. L.; Soles, C. L.; Lenhart, J. L.; Wu, W. L. *J. Vac. Sci. Technol. B* **2001**, *19* (6), 2699–2704.
- (70) Qiu, X. H.; Ediger, M. D. *J. Phys. Chem. B* **2003**, *107* (2), 459–464.
- (71) Reinsberg, S. A.; Qiu, X. H.; Wilhelm, M.; Spiess, H. W.; Ediger, M. D. *J. Chem. Phys.* **2001**, *114* (17), 7299–7302.
- (72) Duenas, J. M. M.; Ribelles, J. L. G. *J. Therm. Anal. Calorim.* **2003**, *72* (2), 695–705.
- (73) Chin, Y. H.; Inglefield, P. T.; Jones, A. A. *Macromolecules* **1993**, *26* (20), 5372–5378.
- (74) Chin, Y. H.; Zhang, C.; Wang, P.; Inglefield, P. T.; Jones, A. A.; Kambour, R. P.; Bendler, J. T.; White, D. M. *Macromolecules* **1992**, *25* (12), 3031–3038.
- (75) Kamath, S. Y.; Arlen, M. J.; Hamilton, W. A.; Dadmun, M. D. *Macromolecules* **2008**, *41* (9), 3339–3348.
- (76) Kamath, S. Y.; Dadmun, M. D. *J. Chem. Phys.* **2006**, *125* (9).
- (77) Arlen, M. J.; Dadmun, M. D.; Hamilton, W. A. *J. Polym. Sci., Part B: Polym. Phys.* **2004**, *42* (17), 3235–3247.
- (78) Arlen, M. J.; Dadmun, M. D. *Polymer* **2003**, *44* (22), 6883–6889.
- (79) Certain commercial equipment and materials are identified in this paper in order to specify adequately the experimental procedure. In no case does such identification imply recommendations by the National Institute of Standards and Technology nor does it imply that the material or equipment identified is necessarily the best available for this purpose.